Translational Oncology
www.transonc.com

Volume 12 Number 5 May 2019 pp. 749–756 749

Arterial Spin Labeling for Glioma Grade Discrimination: Correlations with IDH1 Genotype and 1p/19q Status

Ning Wang, Shu-yi Xie, Hui-ming Liu, Guo-quan Chen and Wei-dong Zhang

Department of Radiology, Sun Yat-sen University Cancer Center, State Key Laboratory of Oncology in South China, Collaborative Innovation Center for Cancer Medicine, 651 Dongfeng East Road, Guangzhou 510060, China

Abstract

Since accurate grading of gliomas has important clinical value, the aim of this study is to evaluate the diagnostic efficacy of perfusion values derived from arterial spin labeling (ASL) to grade gliomas. In addition, the correlation between perfusion and isocitrate dehydrogenase 1 (IDH1) genotypes and chromosome arms 1p and 19q (1p/19q) status of gliomas was assessed. A total of 52 cases of supratentorial gliomas in adults who received ASL imaging were enrolled in this retrospective study. The cerebral blood flow (CBF) images derived from ASL and anatomical maps were normalized to the Montreal Neurological Institute coordinate system and matched. The mean CBF (meanCBF), the maximum CBF (maxCBF), and their relative values (rmeanCBF and rmaxCBF, respectively) were assessed in each case. The tumor grades, IDH1 genotypes, and 1p/19q status were diagnosed according to the 2016 WHO criteria. Receiver operating characteristic curves were performed to assess the efficacy of perfusion parameters for grading. Qualitatively, all gliomas were divided into high- and low-perfusion groups. The crosstabs chi-square test of independence was performed to calculate contingency coefficient (C) and Cramer V coefficient to assess the correlation between perfusion and IDH1 genotypes and 1p/19q status of gliomas. The rmaxCBF showed the best diagnostic efficacy; meanwhile, rmeanCBF had the best specificity for grade discrimination. In astrocytoma, there was a mild correlation between IDH1 genotypes and tumor perfusion with the Cramer's V coefficient of 0.378. There was no significant association between 1p/19q codeletion and perfusion in grade II and III gliomas.

Translational Oncology (2019) 12, 749–756

Introduction

Gliomas are the most common primary intra-axial brain tumors, originated from glial cells. According to the World Health Organization (WHO) classification system [1], gliomas can be classified into four grades: WHO grade I, II, III and IV. WHO grade II gliomas are usually described as low-grade tumors, whereas high-grade gliomas refer to WHO grade III and IV gliomas. The clinical management and prognosis significantly differ for gliomas of different grades and pathological types [2,3]. Patients with low-grade gliomas tend to choose positive treatments and have better compliance. On the contrary, patients with high-grade gliomas are often reluctant to receive aggressive treatments due to their short survival and high relapse rate. Therefore, accurate preoperative grading of gliomas has important clinical value.

According to the 2016 WHO criteria, molecular features have been incorporated into the classification of brain tumors. Especially for diffuse astrocytic and oligodendroglial tumors, isocitrate dehydrogenase (IDH) genotypes and status of chromosome arms 1p and 19q (1p/19q) become important parts for subtyping [1]. IDH mutations that occur in gliomas include IDH1 and IDH2 mutations, with the former accounting for the vast majority [4,5]. Previous studies have shown that the presence or absence of IDH mutation and 1p/19q codeletion affects the prognosis of gliomas [6]. Exploring the

Corresponding author.
E-mail: zhangwd@sysucc.org.cn
Received 8 November 2018; Accepted 21 February 2019

1936-5233/19
https://doi.org/10.1016/j.tranon.2019.02.013

association between radiologic parameters and pathological molecular characteristics of gliomas will enhance the role of imaging techniques in the precision medicine of brain tumors.

Arterial spin labeling (ASL), as a noninvasive perfusion magnetic resonance (MR) imaging technique without administration of exogenous contrast agent, can qualitatively and quantitatively evaluate cerebral blood flow (CBF) whether under physiological or pathological conditions. Several researches have shown that ASL can help discriminate high- and low-grade gliomas [7,8]. Although some studies [9–12] suggested that CBF obtained from ASL may have relationships with histopathologic parameters, such as vascular density and epidermal growth factor receptor status. Few studies focus on the correlations of perfusion with IDH1 genotype and 1p/19q status.

Although ASL can be useful to evaluate the perfusion of gliomas, the low resolution of CBF maps derived from ASL limits its clinical application, especially for quantitative analysis of perfusion. In view of this, our study has adopted a method of normalizing CBF maps and anatomical images into the Montreal Neurological Institute (MNI) coordinate system and mapping the region of interest (ROI) of the whole solid part of the tumor on its anatomical images. More details are described below.

This retrospective study aimed to evaluate the diagnostic efficacy of perfusion parameters derived from ASL for grading gliomas. In addition, we preliminarily explored the association of perfusion parameters with IDH1 genotypes and 1p/19q status of gliomas.

Material and Methods

Subjects

The institutional review board approved this retrospective study. Patient informed consent was waived. We selected patients with untreated brain tumors who performed MR imaging including ASL from October 2015 to January 2018 and then obtained histopathological results through surgical resection in our hospital. There were 58 patients with pathologically confirmed gliomas. Overall, six patients were excluded: three patients less than 18 years old, one patient with the lesion located in the cerebellum, one patient with the angiocentric glioma classified as WHO grade I glioma, and one patient whose ASL images cannot be processed. Finally, a total of 52 cases of supratentorial gliomas in adults who received ASL MR imaging were enrolled in this study.

Imaging Methods

Conventional MR Imaging. MR imaging was performed with a 3.0-T MRI scanner (Discovery 750 W, GE Healthcare) with an 8-channel phased array head coil. Conventional MR imaging sequences included T1-weighted FSE-IR imaging, T2-weighted Propeller imaging, T2-weighted FLAIR imaging (T2FLAIR), and contrast-enhanced FSPGR T1-weighted imaging (ceT1WI) in the axial plane at a slice thickness of 5 mm with 1 mm interval. All the patients performed axial three-dimensional T1-weighted BRAVO imaging (3DT1) at a slice thickness of 4 mm without a gap before gadolinium administration except in four patients in whom 3DT1 was performed after enhancement.

ASL MR Imaging. ASL imaging was obtained by using a three-dimensional pseudocontinuous pulse sequence. Acquisition parameters were as follows: FOV = 240 × 240 mm, TR = 4674 milliseconds, TE = 10.5 milliseconds, post label delay = 1525 milliseconds, slice thickness = 4 mm, slice gap = 0 mm, number of slices = 28, number of excitation = 3, points = 512, arms = 8, and scan time = 4 minutes 31 seconds.

Image Processing and Analysis. The CBF maps derived from ASL were calculated using a 3D ASL package within functool 9.4.05 on the AW VolumeShare 5 (GE Healthcare).

Considering low-resolution of the CBF maps and heterogeneity of participants' images, we adopted a relatively new method to define the ROI.

First, within-subject images matching and spatial normalization to the MNI coordinate system [13] were achieved using SPM 12 (http://www.fil.ion.ucl.ac.uk/spm/). There were some researches using similar normalization methods to study brain diseases [14,15]. To be specific, CBF maps were registered to the corresponding 3DT1 images, and then the two series of images were normalized to the MNI coordinate system through the deformation fields estimated by 3DT1 images. Meanwhile, T2FLAIR and ceT1WI images were normalized by their respective evaluated deformation. All series of normalized images were written with the voxel sizes of 1, 1, and 1 in mm. Afterwards, the normalized CBF maps were registered to the corresponding normalized anatomical maps individually, just like Zeng et al. did [7].

Next, the drawing of ROIs was implemented on a free image analysis software, MRIcron (http://people.cas.sc.edu/rorden/mricron/index.html). The value of ROI on the CBF map which represented the corresponding regional CBF (ml/min/100 g) was extracted using this software.

For quantitative analysis, three ROIs needed to be drawn on the normalized images for each case: 1) A 3D ROI (Figure 1) was delineated on T2FLAIR images to include whole solid part of the tumor, while macroscopic necrosis, gross hemorrhage, large vessels, and edema nearby were excluded referring to all the anatomical images. Then, the 3D ROI was put on the co-registered CBF map, and the mean value extracted from the ROI was recorded as meanCBF of the glioma. 2) The second ROI with a circular appearance was set on the brightest area of the whole tumor on the CBF map, with its voxels varying from 95 to 105. The mean value extracted from it represented maxCBF of the glioma. 3) Another circular ROI with almost the same size as the second ROI was set on the contralateral normal-appearing gray matter at the same plane as or in the vicinity of the second one. The mean value extracted from the third one was recorded as gray matter CBF, which acted as a reference for calculating relative CBF value [7,16]. The relative value of meanCBF (rmeanCBF) and relative value of maxCBF (rmaxCBF) were calculated by dividing meanCBF and maxCBF with gray matter CBF in individual. Both rmeanCBF and rmaxCBF were dimensionless.

For qualitative analysis of perfusion within gliomas, all cases were simply divided into two groups, high- and low-perfusion groups, based on the presence of high perfusion within the tumor on the CBF map. When there was a visible highlight area in the tumor tissue compared to the mirror normal area, the glioma was considered to be a high-perfusion one. If not, it was divided into low-perfusion group.

To assess interobserver agreement, two radiologists were asked to delineate all the ROIs in each case, as well as to divide gliomas into high- and low-perfusion groups. When the two observers drew different conclusions, they need to reassess to reach a consensus result.

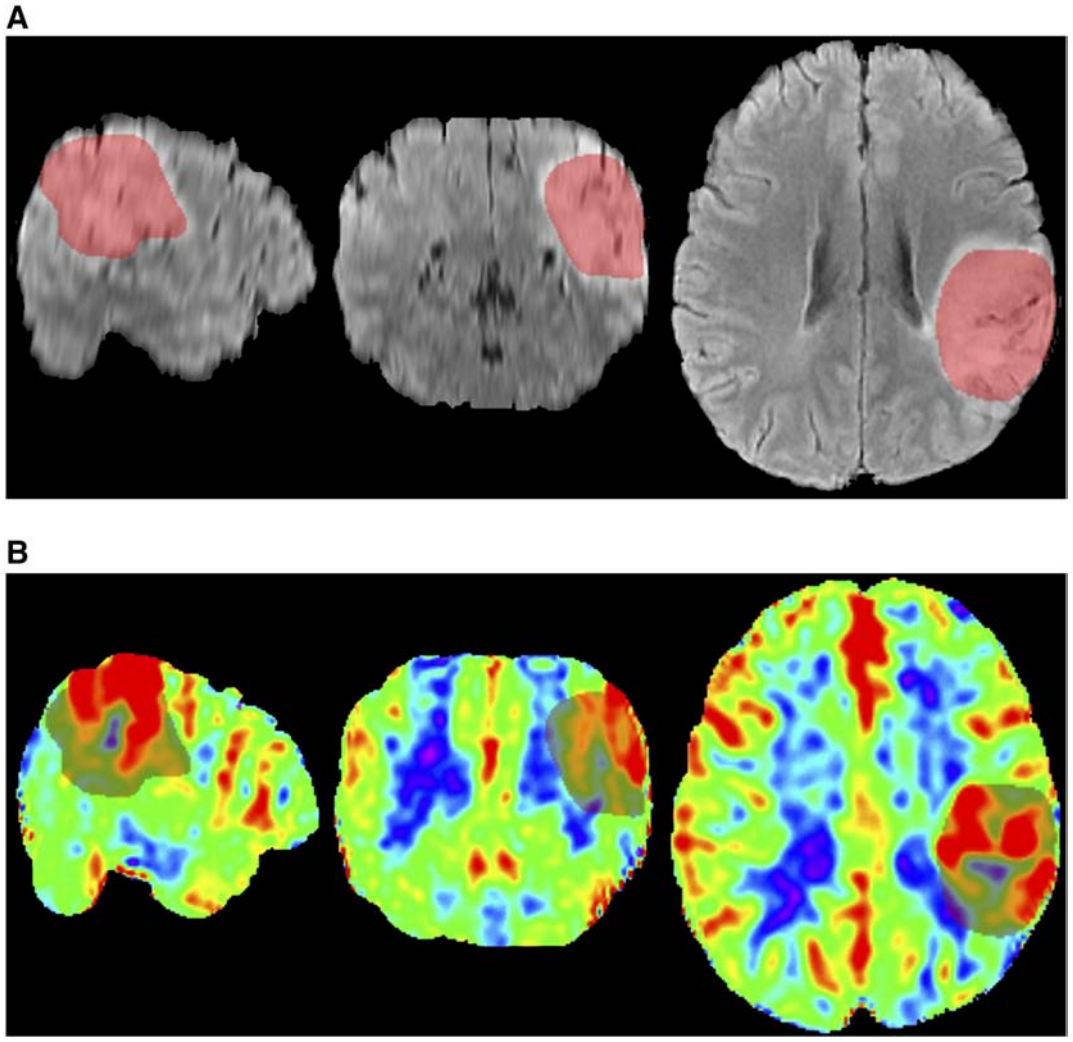

Figure 1. MR images in the MNI coordinate system of a 54-year-old female with diffuse astrocytoma, WHO grade II. T2-weighted FLAIR images (a), in the sagittal, coronal, and axial plane from left to right, show a hyperintense mass covered with a red translucent layer representing a 3D ROI of the whole tumor. The corresponding color-coded CBF maps (b) show lower perfusion of the tumor than the contralateral area since blue represents relatively low perfusion while red represents hyperperfusion.

Histologic Analysis

All cases were diagnosed by the Departments of Pathology and Molecular Diagnostics in our hospital according to the WHO 2016 classification for central nervous system tumors. When different pathological grades were evaluated within different regions of a tumor occasionally, the highest grade was taken. WHO grade II gliomas were divided into low-grade group, whereas high-grade group included WHO grade III and IV gliomas. Molecular markers included IDH1 genotype (IDH1 mutant or wild-type) and 1p/19q status (1p/19q codeleted or non-codeleted). The cases missing molecular information were considered to be not otherwise specified.

Statistical Analysis

Statistical analyses were performed with SPSS (IBM, version 24). For statistical significance, the α level was set at 0.05.

The Shapiro-Wilk normality test was used to test the normality of quantitative data. The absolute and relative CBF values were compared between the high- and low-grade gliomas by using the Mann-Whitney *U* test due to the non-normal distribution of the data. The comparison among gliomas of different WHO grades was implemented by using Kruskal-Wallis test with Bonferroni correction. Receiver operating characteristic (ROC) curves were performed for absolute and relative CBF values to assess the area under the ROC curve (AUC) and find the optimal perfusion parameter and its best cutoff value to discriminate high- and low-grade gliomas.

The quantitative perfusion parameters were compared between IDH1 mutant and wild-type groups, and between 1p/19q codeleted and non-codeleted group by using the Mann-Whitney *U* test or *t* test according to the normality of data. For qualitative analysis, crosstabs chi-square test of independence was performed to calculate contingency coefficient (C) and Cramer V coefficient to assess the correlation between perfusion parameters and IDH1 genotypes and 1p/19q status of gliomas.

Intraclass correlation efficient (ICC) was calculated to assess interobserver agreement for quantitative perfusion parameters. For qualitative analysis, Kappa value was used to evaluate the consistency between the two observers.

Table 1. Histopathological Characteristics of Gliomas

WHO Grade	Histopathological Type	No. of Patients	No. of IDH1 Mutant /wild-Type	No. of 1p/19q Codeleted/Non-Codeleted
I	Angiocentric glioma	1	0/1	0/1
II	Ganglioglioma	1	0/1	0/1
	Pleomorphic xanthoastrocytoma	1	1/0	0/1
	Diffuse astrocytoma	10	10/0	0/8, NOS 2
	Oligodendroglioma	3	2/1	3/0
	Overall	15	13/2	3/10, NOS 2
III	Anaplastic astrocytoma	6	5/1	0/6
	Anaplastic oligodendroglioma	6	4/0, NOS 2	6/0
	Granular cell astrocytoma	1	0/1	0/1
	Overall	13	9/2, NOS 2	6/7
IV	Glioblastomas	24	3/21	0/24

NOS: the abbreviation of not otherwise specified. The number behind NOS referred to the number of cases that did not have clear information of IDH1 genotype or 1p/19q status.

Results

Patients' Characteristics

Among the 52 patients included, there were 24 men and 28 women. The median age of the patients was 48 years (range 23-81 years). The pathological types and grades, as well as IDH1 genotypes and 1p/19q status of gliomas were summarized in Table 1.

Consistency of Perfusion Values

The ICCs of all the quantitative parameters were listed in Table 2. All the values measured by the two radiologists showed good consistency. We chose the first observer's values for analysis. As for the qualitative analysis of perfusion, the observers showed strong consistency (Kappa value = 0.813).

Diagnostic Efficacy of CBF for Grading

ASL could help discriminate high-grade gliomas (n = 37) from low-grade gliomas (n = 16). All the perfusion values showed statistically different between high-grade and low-grade gliomas.

The maxCBF [median, 101.29; interquartile range (IQR), 80.71-156.10 vs median, 57.11; IQR, 44.68-80.57 ml/min/100 g; P = .003], the rmaxCBF [median, 2.12; IQR, 1.61-2.84 vs median, 1.14; IQR, 0.93-1.55; P = .001], the meanCBF [median, 48.80; IQR, 40.46-63.79 vs median, 37.50; IQR, 27.03-54.61 ml/min/100 g; P = .033], and the rmeanCBF [median, 0.96; IQR, 0.78-1.30 vs median, 0.73; IQR, 0.54-0.87; P = .006] in high-grade group were significantly higher than in low-grade group.

ROC analysis for perfusion parameters was performed to assess the discrimination efficiency between high- and low-grade gliomas, and the results were presented in Figure 2 and Table 3. Among the parameters, rmaxCBF showed the best identification ability with the optimal cutoff value of 1.25 based on the maximum Youden index. Meanwhile, rmeanCBF showed a higher specificity (86.7%) than other parameters.

Diagnostic Efficacy of CBF Among Subgroups

Intergroup analysis among three subgroups, WHO grade II, III, and IV gliomas, was performed to assess the ability of ASL to separate different grade gliomas (Figure 3).

Table 2. Intraclass Correlation Efficient (ICC) for Quantitative Perfusion Parameters

	MeanCBF	MaxCBF	RmeanCBF	RmaxCBF	Gray matter CBF
ICC	0.979	0.982	0.907	0.954	0.881
P value	.000	.000	.000	.000	.000

Except the meanCBF, other parameters showed significant difference among three subgroups. The rmaxCBF in WHO grade II gliomas was significantly lower than that in grade III (P = .001) and IV subgroups (P = .007). However, none of these parameters could differentiate grade III from IV gliomas.

Qualitative Assessment of Perfusion

To confirm the reliability of qualitative assessment, four quantitative CBF values were compared between high- and low-perfusion gliomas. All the perfusion parameters showed significantly differences (P<.001) between the two groups.

Correlation of Perfusion with IDH1 Genotype

Regardless of grades and 1p/19q status, rmeanCBF was lower in IDH1 mutant group than in IDH1 wild-type group (P = .047); the other parameters did not show statistical differences between IDH1 mutant and wild-type groups (P = .097, .455, and .282, respectively,

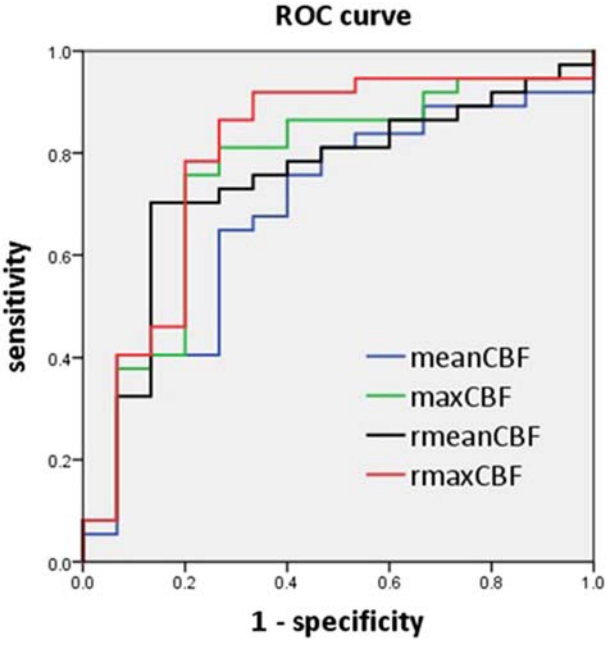

Figure 2. ROC curve for meanCBF, maxCBF, rmeanCBF, and rmaxCBF in distinguishing high- from low-grade gliomas. ROC curve: receiver operating characteristic curve; meanCBF: mean CBF (ml/min/100 g); maxCBF: maximum CBF (ml/min/100 g); rmeanCBF: relative value of meanCBF (dimensionless); rmaxCBF: relative value of maxCBF (dimensionless).

Table 3. Diagnostic Performance of Perfusion Parameters for Distinguishing High- from Low-Grade Gliomas

Parameters	AUC	Cutoff Value	Sensitivity	Specificity
meanCBF	0.690	44.59 (ml/min/100 g)	0.649	0.733
maxCBF	0.762	81.07 (ml/min/100 g)	0.757	0.800
rmeanCBF	0.744	0.89	0.703	0.867
rmaxCBF	0.798	1.25	0.865	0.733

for meanCBF, maxCBF, and rmaxCBF). For qualitative analysis, tumor perfusion showed a mild association with IDH1 genotypes (C = 0.304, Cramer V = 0.319, P = .024).

There were only two cases with IDH1 wild-type gliomas in the low-grade group, and there were 12 cases with IDH1 mutant and 23 cases with IDH1 wild-type gliomas in the high-grade group. We only analyzed the perfusion of gliomas with different IDH1 genotype in the high-grade group. However, none of the perfusion parameters showed statistical differences between IDH1 mutant and wild-type

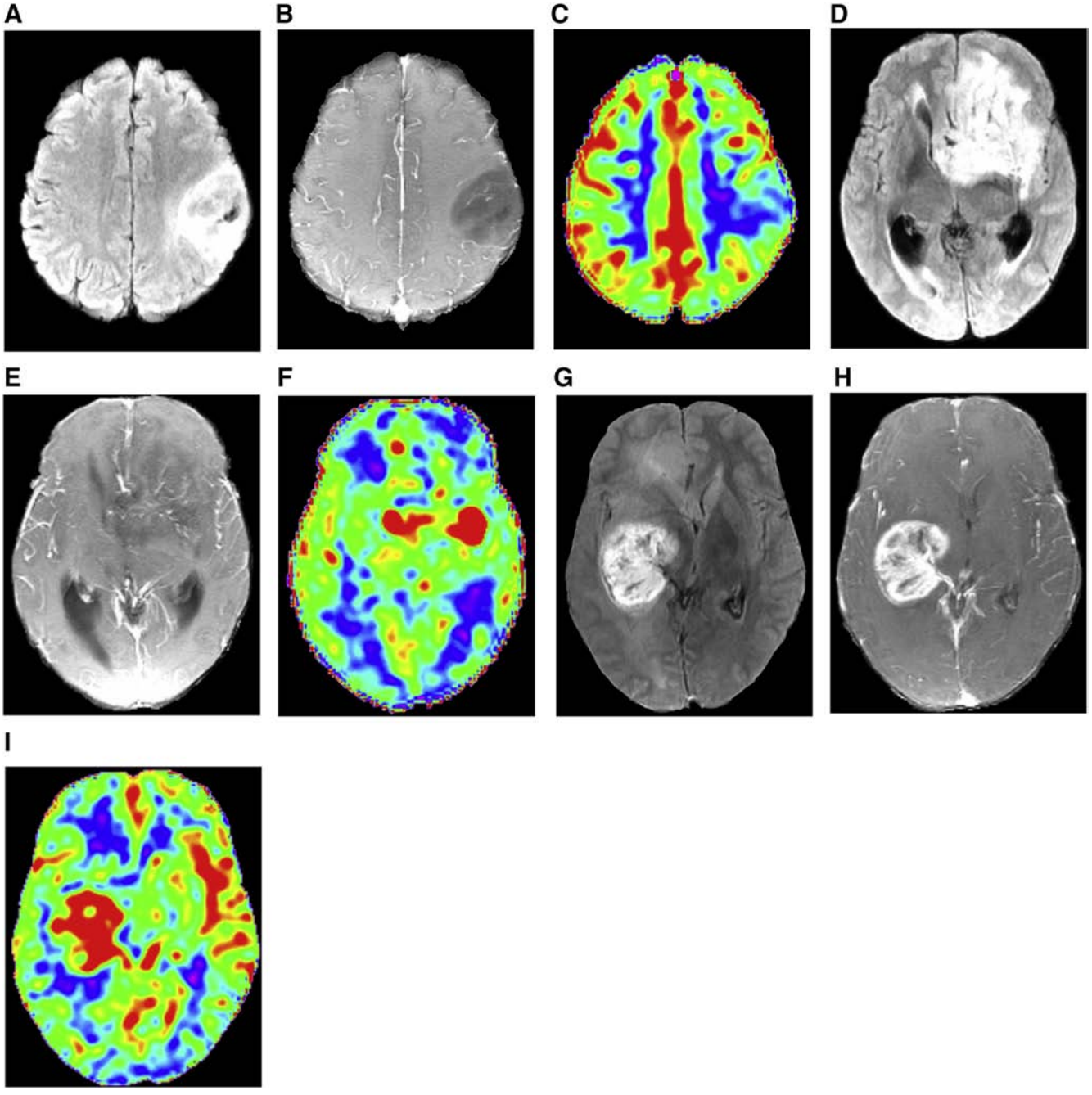

Figure 3. Representative cases for WHO grade II (a, b, c), III (d, e, f), and IV (g, h, i) gliomas with aligned T2FLAIR (a, d, g), ceT1WI (b, e, h), and corresponding CBF maps (c, f, i).A 31-year-old female with diffuse astrocytoma (a, b, c). T2FLAIR (a) shows a mildly high intense mass with obscure boundary; meanwhile, ceT1WI (b) shows no obvious enhancement. The corresponding CBF map (c) show hypoperfusion of the tumor. A 50-year-old female with anaplastic oligodendroglioma (d, e, f). The tumor shows hyperintensity on T2FLAIR (d), foci of enhancement on ceT1WI (e), and heterogeneous hyperperfusion on CBF map (f). A 34-year-old male with glioblastoma (g, h, i). The tumor shows heterogeneous hyperintensity on T2FLAIR (g), obvious enhancement on ceT1WI (h), and hyperperfusion almost in all tumor zones on CBF map (f).

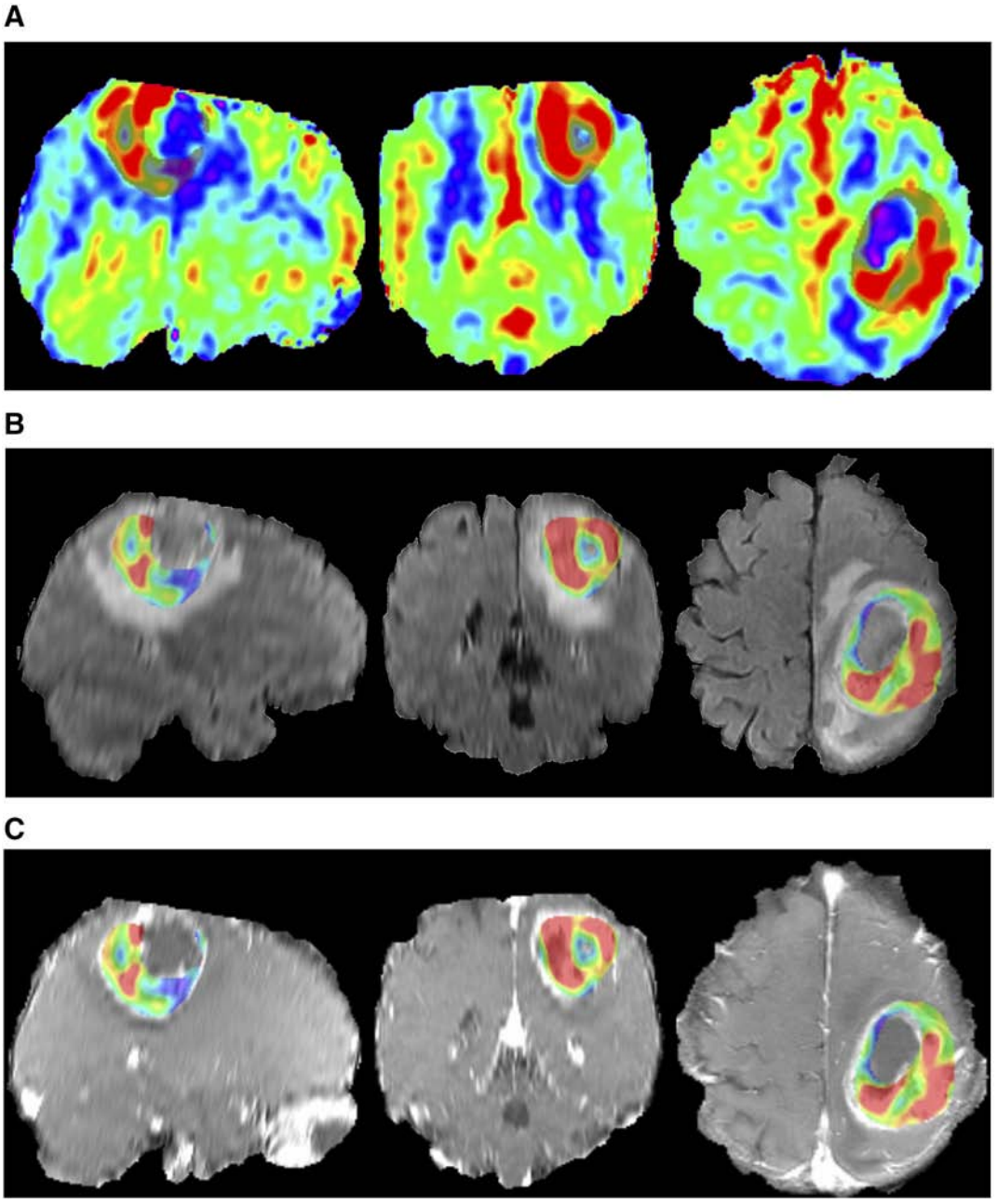

Figure 4. MR images and the 3D tumor mask of a 47-year-old female with IDH1–wild-type glioblastoma. The color-coded CBF maps (a) in the sagittal, coronal, and axial plane from left to right show a thick and irregular ring hyperperfusion of the tumor covered with a translucent layer representing the 3D ROI. The 3D tumor mask extracted from CBF maps is exactly projected on to the corresponding T2FLAIR (b) and ceT1WI (c).

gliomas in the high-grade group. For qualitative analysis, tumor perfusion failed to yield a significant association with IDH1 genotypes using a Fisher's exact test.

In a sample of astrocytoma (WHO grade II, III, and IV), that is to say, excluding oligodendrogliomas and one case of ganglioglioma, the rmeanCBF [median, 0.76; IQR, 0.54-0.92 vs median, 0.96; IQR, 0.80-1.41; $P = .010$] in IDH1 mutant gliomas was significantly lower than that in IDH1 wild-type gliomas. Other perfusion parameters failed to show significant differences between the two groups. A moderate correlation was shown between perfusion and IDH1 genotype of gliomas (C = 0.354, Cramer V = 0.378, $P = .014$).

Correlation of Perfusion with 1p/19q Status

As a characteristic feature of oligodendroglioma, 1p/19q codeletion was shown in three patients with oligodendroglioma and six patients with anaplastic oligodendroglioma.

Considering the distribution of 1p/19q codeletion, we analyzed the correlation between perfusion and 1p/19q status in WHO grade II and III gliomas.

The rmaxCBF in the 1p/19q codeleted group was significantly higher than that in the non-codeleted group [median, 2.65; IQR, 1.80-3.15 vs median, 1.24; IQR, 1.00-1.88; $P = .042$]. The rmeanCBF in the 1p/19q codeleted group was also higher than that in the non-codeleted group [median, 1.16; IQR, 0.78-1.24 vs

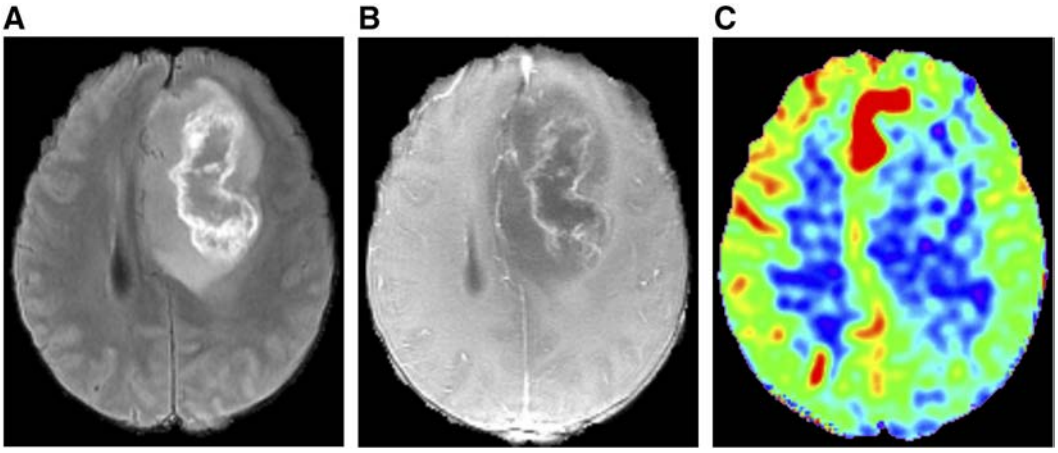

Figure 5. A 46-year-old male with IDH1-mutant glioblastoma. T2FLAIR (a) shows a heterogeneous hyperintensity mass, with inner linear higher intensity and central hypointensity representing necrosis. CeT1WI (b) shows irregular ring enhancement with a shaggy inner margin in the same part as linear higher intensity on T2FLAIR. The corresponding CBF map (c) shows no obvious hyperperfusion in the tumor location except for the zone near the midline of brain.

median, 0.85; IQR, 0.69-0.96; P = .048], while meanCBF and maxCBF did not significantly differ between the two groups.

As for WHO grade II and III gliomas, there was no significant association between 1p/19q status and tumor perfusion using a Fisher's exact test. (C = 0.272, Cramer V = 0.282, P = .355).

Discussion

Considering the overlaps of conventional anatomical imaging findings between high- and low-grade gliomas, functional MR imaging techniques, such as ASL, have been applied to the differential diagnosis. In this study, tumor perfusion values, especially rmaxCBF, demonstrated good diagnostic performance for grading gliomas. The result is consistent with previous studies [7,17].

Previous studies declared that rmaxCBF rather than rmeanCBF of gliomas had higher diagnostic efficiency for distinguishing high- from low-grade gliomas [18,19]. Therefore, many researches concerning perfusion of brain tumors focused on the maxCBF or rmaxCBF [7,9,16]. To our knowledge, although there were a few studies evaluating the value of meanCBF in brain tumor, the ROIs used for measurement did not include the whole tumor tissue [16,20,21]. Therefore, we preferred to contain total solid part of a tumor, in another word, create a 3D tumor mask (Figure 4), to calculate the meanCBF. The measurement might be more representative and was also used in a previous study [18]. This 3D ROI has also been used to assess tumor volume [22] and to measure apparent diffusion coefficient histogram [23]. In our study, rmeanCBF had a higher specificity than other parameters as an index of differential diagnosis.

In our sample, WHO grade III gliomas seemed to have higher perfusion than the grade IV gliomas, although it was not statistically significant. The result was contrary to the previous report [7]. The possible reasons may include the following points: 1) Anaplastic oligodendrogliomas accounted for nearly 50% of cases in the WHO grade III group. Some studies believed that oligodendrogliomas preferred to be high perfusion [7,24,25]. 2) Some glioblastomas actually did not display high perfusion on CBF maps. The variable perfusion patterns of glioblastomas have also been reported by Qiao et al. [11]. The expression of hypoxia-related markers and necrosis in glioblastomas made the tumor perfusion more complicated [26–28]. 3) Sometimes, the margins of glioblastomas were hard to be clearly defined. When the whole solid part of the tumor was included to assess CBF, it was inevitable to bring in a few hypoperfusion edema areas mistaken as tumor tissue. Korkolopoulou et al. [29] found that microvessel density was higher in WHO grade III astrocytomas than in grade IV ones without statistics significance. The result was consistent with our finding, given the positive correlation between perfusion and vascular density [9,10].

The implementation of reproducible quantitative measurement of CBF depends strongly on exact and unified delineation of ROIs. We tried to normalize all images to the MNI coordinate system and then match anatomic maps and CBF maps individually. A 3D ROI was drawn including all solid tumor tissues to calculate meanCBF mainly based on T2FLAIR rather than ceT1WI due to inconsistency between high-perfusion zone and enhanced zone in gliomas [30]. Moreover, the ROIs of tumor maximum perfusion zone and contralateral gray matter were kept to a uniform size. Nevertheless, it is still a challenge to achieve uniform measurement of CBF and to obtain repeatable CBF cutoff value, considering relative low resolution of CBF maps.

In the practical clinical application, radiologists usually simply divide gliomas into high- and low-perfusion groups. Our study verified the reliability of this simple classification. Other qualitative classifications of CBF maps have also been used in gliomas and meningiomas [11,31,32].

A mild correlation was showed between perfusion and IDH1 genotype regardless of grades and 1p/19q status, and a similar result was also found in astrocytoma. It deserves to be explored whether ASL can be a useful imaging technique to assess IDH1 genotype before operation. Considering the small proportion of IDH1-mutant ones in high-grade gliomas (Figure 5) and IDH1–wild-type ones in low-grade gliomas, we can try to expand sample size or balance the proportion of two IDH1 genotype groups in the same grade gliomas in the next step.

Some published literatures believed that oligodendrogliomas tended to be high perfusion [24,33]. Since 1p/19q codeletion is a distinguishing feature of oligodendrogliomas, our study explored the correlation between 1p/19q codeletion and perfusion. However, there was no clear correlation between them.

Therefore, there are still many things deserved to be done in further researches. First, we need to search a more accurate and subjective segmentation of gliomas on the CBF maps, and it will be more convincing to verify the CBF cutoff values in another sample. Second, the qualitative value of ASL needs to be explored through different sorting schemes. Third, it will be very valuable to enlarge the sample size to explore the association of perfusion with IDH1 genotype and 1p/19q status. Finally, ASL combining other imaging techniques [34,35] may be more conducive to imaging diagnosis of glioma.

Conclusions

ASL can help grading gliomas. The rmaxCBF displays best diagnostic performance; meanwhile, rmeanCBF has a higher specificity to distinguish high- from low-grade gliomas. Preliminary results showed a mild correlation between IDH1 genotypes and perfusion in astrocytoma, but no significant association was found between 1p/19q status and perfusion of gliomas.

Acknowledgements

The scientific guarantor of this publication is Wei-dong Zhang, MD. The authors declared no conflicts of interest. This research did not receive any specific grant from funding agencies in the public, commercial, or not-for-profit sectors.

References

[1] Louis DN, Perry A, and Reifenberger G, et al (2016). The 2016 World Health Organization classification of tumors of the central nervous system: a summary. *Acta Neuropathol* **131**, 803–820.

[2] Weller M, van den Bent M, and Tonn JC, et al (2017). European Association for Neuro-Oncology (EANO) guideline on the diagnosis and treatment of adult astrocytic and oligodendroglial gliomas. *Lancet Oncol* **18**, e315–e329.

[3] Rasmussen BK, Hansen S, and Laursen RJ, et al (2017). Epidemiology of glioma: clinical characteristics, symptoms, and predictors of glioma patients grade I-IV in the the Danish Neuro-Oncology Registry. *J Neuro-Oncol* **135**, 571–579.

[4] Cohen A, Holmen S, and Colman H (2013). IDH1 and IDH2 mutations in gliomas. *Curr Neurol Neurosci Rep* **13**, 345.

[5] Chen N, Yu T, and Gong J, et al (2016). IDH1/2 gene hotspot mutations in central nervous system tumours: analysis of 922 Chinese patients. *Pathology* **48**, 675–683.

[6] Eckel-Passow JE, Lachance DH, and Molinaro AM, et al (2015). Glioma groups based on 1p/19q, IDH, and TERT promoter mutations in tumors. *N Engl J Med* **372**, 2499–2508.

[7] Zeng Q, Jiang B, Shi F, Ling C, Dong F, and Zhang J (2017). 3D Pseudocontinuous arterial spin-labeling MR imaging in the preoperative evaluation of gliomas. *AJNR Am J Neuroradiol* **38**, 1876–1883.

[8] Kong L, Chen H, Yang Y, and Chen L (2017). A meta-analysis of arterial spin labelling perfusion values for the prediction of glioma grade. *Clin Radiol* **72**, 255–261.

[9] Kikuchi K, Hiwatashi A, and Togao O, et al (2017). Correlation between arterial spin-labeling perfusion and histopathological vascular density of pediatric intracranial tumors. *J Neuro-Oncol* **135**, 561–569.

[10] Ningning D, Haopeng P, and Xuefei D, et al (2017). Perfusion imaging of brain gliomas using arterial spin labeling: correlation with histopathological vascular density in MRI-guided biopsies. *Neuroradiology* **59**, 51–59.

[11] Qiao X, Ellingson B, and Kim H, et al (2015). Arterial spin-labeling perfusion MRI stratifies progression-free survival and correlates with epidermal growth factor receptor status in glioblastoma. *AJNR Am J Neuroradiol* **36**, 672–677.

[12] Yoo R, Choi S, and Cho H, et al (2013). Tumor blood flow from arterial spin labeling perfusion MRI: a key parameter in distinguishing high-grade gliomas from primary cerebral lymphomas, and in predicting genetic biomarkers in high-grade gliomas. *J Magn Reson Imaging* **38**, 852–860.

[13] Chau W and McIntosh A (2005). The Talairach coordinate of a point in the MNI space: how to interpret it. *NeuroImage* **25**, 408–416.

[14] Wang DJ, Alger JR, and Qiao JX, et al (2013). Multi-delay multi-parametric arterial spin-labeled perfusion MRI in acute ischemic stroke — comparison with dynamic susceptibility contrast enhanced perfusion imaging. *Neuroimage Clin* **3**, 1–7.

[15] Wang DJ, Alger JR, and Qiao JX, et al (2012). The value of arterial spin-labeled perfusion imaging in acute ischemic stroke: comparison with dynamic susceptibility contrast-enhanced MRI. *Stroke* **43**, 1018–1024.

[16] Dangouloff-Ros V, Deroulers C, and Foissac F, et al (2016). Arterial spin labeling to predict brain tumor grading in children: correlations between histopathologic vascular density and perfusion MR imaging. *Radiology* **281**, 553–566.

[17] Ma H, Wang Z, and Xu K, et al (2017). Three-dimensional arterial spin labeling imaging and dynamic susceptibility contrast perfusion-weighted imaging value in diagnosing glioma grade prior to surgery. *Exp Ther Med* **13**, 2691–2698.

[18] Wolf R, Wang J, and Wang S, et al (2005). Grading of CNS neoplasms using continuous arterial spin labeled perfusion MR imaging at 3 Tesla. *J Magn Reson Imaging* **22**, 475–482.

[19] Khashbat D, Harada M, and Abe T, et al (2017). Diagnostic performance of arterial spin labeling for grading nonenhancing astrocytic tumors. *Magn Reson Med Sci*. https://dx.doi.org/10.2463/mrms.mp.2017-0065.

[20] Yamashita K, Yoshiura T, and Hiwatashi A, et al (2012). Arterial spin labeling of hemangioblastoma: differentiation from metastatic brain tumors based on quantitative blood flow measurement. *Neuroradiology* **54**, 809–813.

[21] Kang KM, Sohn CH, and You SH, et al (2017). Added value of arterial spin-labeling MR imaging for the differentiation of cerebellar hemangioblastoma from metastasis. *AJNR Am J Neuroradiol* **38**, 2052–2058.

[22] Ganbold MMD, Harada MMDP, Khashbat DMDP, Abe T, Md P, Kageji TMDP, and Nagahiro SMDP (2017). Differences in high-intensity signal volume between arterial spin labeling and contrast-enhanced T1-weighted imaging may be useful for differentiating glioblastoma from brain metastasis. *J Med Investig* **64**, 58–63.

[23] Surov A, Ginat DT, and Lim T, et al (2018). Histogram analysis parameters apparent diffusion coefficient for distinguishing high and low-grade meningiomas: a multicenter study. *Transl Oncol* **11**, 1074–1079.

[24] Cha S, Tihan T, and Crawford F, et al (2005). Differentiation of low-grade oligodendrogliomas from low-grade astrocytomas by using quantitative blood-volume measurements derived from dynamic susceptibility contrast-enhanced MR imaging. *AJNR Am J Neuroradiol* **26**, 266–273.

[25] Sunwoo L, Choi SH, and Yoo RE, et al (2015). Paradoxical perfusion metrics of high-grade gliomas with an oligodendroglioma component: quantitative analysis of dynamic susceptibility contrast perfusion MR imaging. *Neuroradiology* **57**, 1111–1120.

[26] Mayer A, Schneider F, Vaupel P, Sommer C, and Schmidberger H (2012). Differential expression of HIF-1 in glioblastoma multiforme and anaplastic astrocytoma. *Int J Oncol* **41**, 1260–1270.

[27] Evans S, Jenkins K, and Jenkins W, et al (2008). Imaging and analytical methods as applied to the evaluation of vasculature and hypoxia in human brain tumors. *Radiat Res* **170**, 677–690.

[28] Ponte K, Berro D, and Collet S, et al (2017). In vivo relationship between hypoxia and angiogenesis in human glioblastoma: a multimodal imaging study. *J Nucl Med* **58**, 1574–1579.

[29] Korkolopoulou P, Patsouris E, and Kavantzas N, et al (2002). Prognostic implications of microvessel morphometry in diffuse astrocytic neoplasms. *Neuropathol Appl Neurobiol* **28**, 57–66.

[30] Abe T, Mizobuchi Y, and Sako W, et al (2015). Clinical significance of discrepancy between arterial spin labeling images and contrast-enhanced images in the diagnosis of brain tumors. *Magn Reson Med Sci* **14**, 313–319.

[31] Sunwoo L, Yun TJ, and You SH, et al (2016). Differentiation of glioblastoma from brain metastasis: qualitative and quantitative analysis using arterial spin labeling MR imaging. *PLoS One* **11**, e0166662.

[32] Qiao XJ, Kim HG, and Wang DJJ, et al (2017). Application of arterial spin labeling perfusion MRI to differentiate benign from malignant intracranial meningiomas. *Eur J Radiol* **97**, 31–36.

[33] Narang J, Jain R, and Scarpace L, et al (2011). Tumor vascular leakiness and blood volume estimates in oligodendrogliomas using perfusion CT: an analysis of perfusion parameters helping further characterize genetic subtypes as well as differentiate from astroglial tumors. *J Neuro-Oncol* **102**, 287–293.

[34] Jiang S, Zou T, and Eberhart C, et al (2017). Predicting IDH mutation status in grade II gliomas using amide proton transfer-weighted (APTw) MRI. *Magn Reson Med* **78**, 1100–1109.

[35] Zhang B, Chang K, and Ramkissoon S, et al (2017). Multimodal MRI features predict isocitrate dehydrogenase genotype in high-grade gliomas. *Neuro-Oncology* **19**, 109–117.